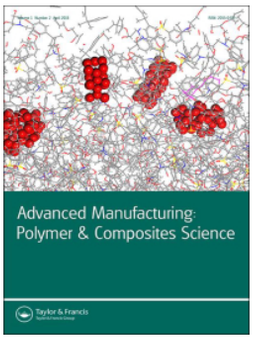

Taylor & Francis
Taylor & Francis Group

Advanced Manufacturing: Polymer & Composites Science

ISSN: (Print) (Online) Journal homepage: https://www.tandfonline.com/loi/yadm20

Thickness variation in contoured composite parts by vacuum infusion

Patricio Martinez, Bo Jin & Steven Nutt

To cite this article: Patricio Martinez, Bo Jin & Steven Nutt (2023) Thickness variation in contoured composite parts by vacuum infusion, Advanced Manufacturing: Polymer & Composites Science, 9:1, 2279604, DOI: 10.1080/20550340.2023.2279604

To link to this article: https://doi.org/10.1080/20550340.2023.2279604

ADVANCED MANUFACTURING: POLYMER & COMPOSITES SCIENCE
2023, VOL. 9, NO. 1, 2279604
https://doi.org/10.1080/20550340.2023.2279604

Taylor & Francis
Taylor & Francis Group

Thickness variation in contoured composite parts by vacuum infusion

Patricio Martinez, Bo Jin and Steven Nutt

M. C. Gill Composites Center, University of Southern CA, Los Angeles, CA, USA

ABSTRACT

Contoured laminates were produced by vacuum infusion (VI), and thickness variations were monitored dynamically as a function of process parameters. Process simulations were performed using finite element software (PAM-RTM), and predictions of thickness along the length of the laminate were compared with dynamic measurements. Initial simulations approximated the effects of corners on preform deformation and fabric draping behavior. Subsequent modifications to the simulation geometry and material properties were implemented to increase accuracy and more closely match experimental measurements. User-defined geometry (UDG) simulations were used to predict both the maximum corner deviation and the area of corner deviation with greater accuracy. The present study demonstrates a workflow for use of analytical tools to design and control vacuum infusion processes. The workflow leverages process monitoring and modified process simulation tools to provide insight into parametric effects and to guide process modifications to reduce product variability.

GRAPHICAL ABSTRACT

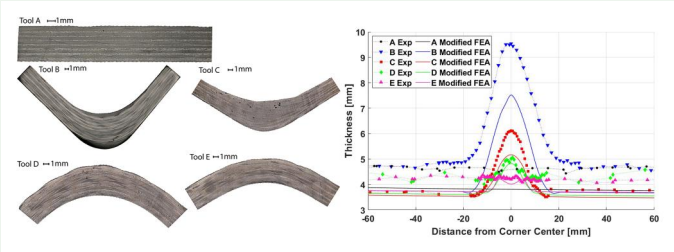

ARTICLE HISTORY
Received 11 July 2023
Accepted 30 October 2023

KEYWORDS
Vacuum infusion; thickness deviation; contoured laminates; finite element analysis

Introduction

Thickness variations commonly arise in composite parts produced by VI, yet the evolution of such defects and the effects of basic process parameters are not fully understood. The present study addresses this gap in understanding and demonstrates a practical workflow that leverages process monitoring, material characterization, and process simulations. Laminate thickness variations are monitored along the length of V-shaped parts produced *via* VI, then compared with results of process simulations conducted using commercial software (PAM-RTM). The effects of variations to geometry and material properties were explored in the context of process simulations in an effort to accurately account for fiber bridging at corners. The investigation demonstrates how process monitoring can be used effectively in coordination with process simulation to understand and control a common defect in VI parts.

VI is a cost-effective method to produce large composite parts such as wind blades and boat hulls, although there is also potential to use the method to produce aerospace parts comprised of carbon fiber reinforced polymer (CFRP) composites [1,2]. VI relies on a relatively small pressure difference to draw resin into a fiber bed that lies between a rigid tool on one side and a flexible vacuum bag on the other. The pressure difference between the resin reservoir at the inlet and the vacuum at the outlet generally induces a gradient in thickness and fiber volume fraction along the part length [3–5].

The presence of corner contours in parts generally causes variations in local thickness in most CFRP production processes, including VI [6–8]. Depending on the curvature of the tool, thickness can increase or decrease at the corner due to reduction or augmentation of the compaction force over the arc. As permeability depends on fiber volume fraction [9,10], local thickness changes result in

CONTACT Patricio Martinez mart136@usc.edu M. C. Gill Composites Center, University of Southern CA, Los Angeles, CA, USA

variations in flow behavior during infusion, as well as dimensional differences once a part is cured [11].

To predict thickness variations before producing a part, process simulation tools for resin infusion processes can be employed [12–15]. This practice has led to development of software dedicated to finite element simulations of flow processes in porous media. Such software can be used to determine appropriate inlet and outlet positions and timing sequences to ensure full saturation, minimize fill times [16], and determine if a reinforcement-resin coupling is compatible with infusion [17]. The process simulation software used in this study (PAM-RTM, ESI) is widely used in industry, and has been used to accurately predict the thickness gradients, mostly in flat laminates [4].

In this study, we demonstrate a method for process simulation to predict thickness deviations in contoured parts produced by VI. In conjunction with this method, we deploy process monitoring to monitor thickness deviations during infusion. These coordinated activities can be used to prevent defects, particularly those associated with thickness variation. Application of process simulations coordinated with process monitoring can be used to maintain geometric specifications, increase geometric tolerances, and reduce part scrap. Flow simulations are widely used in industry for various purposes, but rarely coordinated with process monitoring. The method demonstrated in this work highlights the importance of preform-tool compatibility and the deviations in laminate geometry that typically arise from fabric bridging and inter-ply slippage.

Experimental methods

Thickness variations were measured in VI parts produced on tools with concave and convex corners. A laser displacement system was used to measure laminate thickness during infusion. Following cure, the laminates were sectioned to measure the thickness of the centerline cross-section.

Software (PAM-RTM) was used to simulate infusion for a wide range of corner geometries, including those matching the experimental parts. Analysis revealed that the standard procedure did not adequately account for all corner effects and required modification. The compression response and surface profile of the fabric were measured on specific tool geometries and used to generate a second set of User Defined Geometry (UDG) simulations. Using these UDG's, simulations predicted thickness deviations at the corner much more accurately, both in terms of magnitude and the affected area.

Fabric characterization

Triaxial carbon fabric with a high areal weight (A&P Technologies, QISO-H-48) was selected based on compatibility with VI and the selected resin [17]. General properties are listed in Table 1. The areal weight, braid angle, and thickness were provided by the manufacturer and independently verified. The volumetric density was measured using a gas pycnometer (Micromeritics, Accupyc 1330).

A single ply of the fabric was compressed at 1 µm per second using a rheometer (Texas Instruments, AR2000ex), chosen for its high accuracy in position and force data to obtain stress versus strain compression data for the fabric, for use in the initial simulations. The results of this test is shown in Figure 1. Given the multiple compressions done on the fabric during vacuum leak testing, the second compression was selected as the stress versus strain response for the fabric.

Permeability values of the fabric were measured using a radial infusion set-up, following the same procedure of a previous study [17]. A $[0]_4$ stack of 203.2 mm square plies was sandwiched between aluminum and acrylic tool plates. Plastic shims positioned around the plies were used as spacers to control thickness, with the entire assembly being sealed in a vacuum bag. The test was repeated at least four times for each thickness spacing.

$$V_f = \frac{N \cdot \rho_A}{h \cdot \rho_V} \tag{1}$$

Table 1. Properties of the triaxial fabric.

Property	Value	Units
Areal weight	536	[g/m^2]
Tow angles	0/+60/−60	[°]
Thickness @ 55% V_f	0.5334	[mm]
Density	1.6742×10^6	[g/m^3]

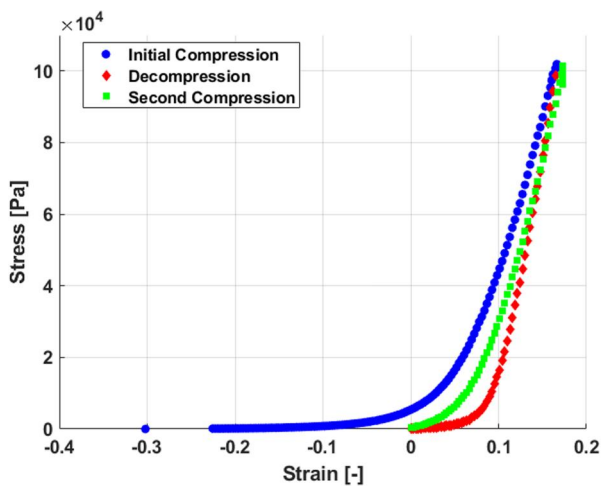

Figure 1. Compression stress versus strain response for a single ply of fabric.

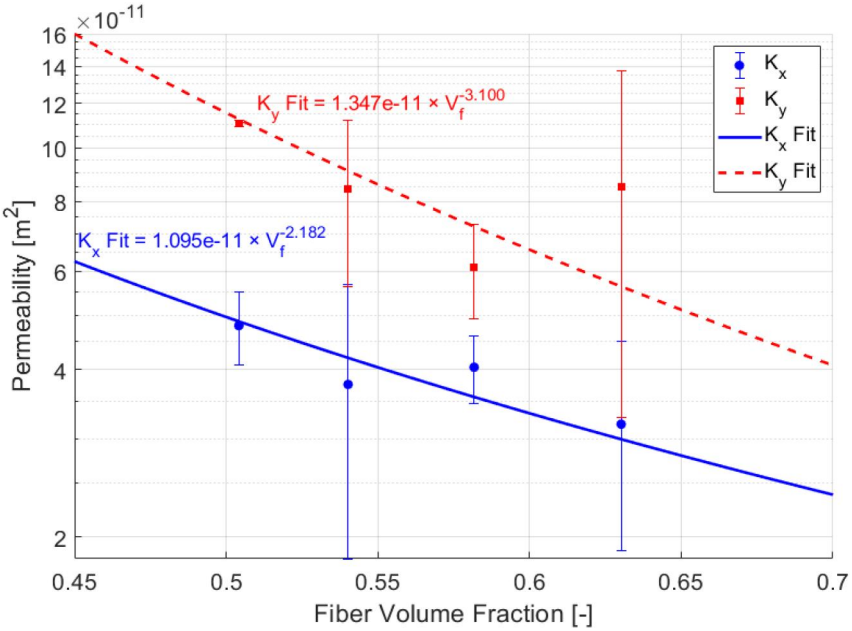

Figure 2. Permeability versus fiber volume fraction in *x*- and *y*-directions for the triaxial fabric.

Table 2. Tool configurations used for experimental trials.

	Tool curvature [–]	Corner angle [°]	Corner radius [mm]
A	Flat	N/A	N/A
B	Concave	90	10
C	Concave	60	10
D	Convex	90	15
E	Convex	60	15

Permeability tests were performed using different spacer thickness values. Employing the number of plies N, the areal weight ρ_A, the density ρ, and the thickness h, the volume fraction was obtained for each test *via* Equation (1). Following the procedure of Chan and Huang [18] the x- and y-directional (0° and 90°) radii of the flow front captured in each image were used to obtain in-plane permeability values for the fabric at each volume fraction. An exponential decay curve was fitted to the data, as shown in Figure 2, as this relation is required for the process simulation. The error bars were significant, as expected, due to the high variability and noise intrinsic to fabric and fabric permeability measurements [19,20].

Laminate production

Laminates were produced using 305×203 mm plies, following an $[0]_8$ layup sequence, selected due to the quasi-isotropic nature of the fabric. Standard VI layup procedure was followed, using conventional consumables. A 25.4 mm gap was cut into the centerline of the flow media to permit direct observation of the laminate surface. Five distinct tool configurations were used (Table 2). For contoured tool configurations (B-E), the fabric was first stacked, then placed at the corner and allowed to drape onto the tool. The fabric was infused with epoxy resin and hardener (FibreGlast 4500 and 4570). Resin was allowed to infuse until steady flow was reached in the outlet line, at which point the inlet and outlet lines were sealed. The parts were subsequently cured at room temperature according to supplier guidelines.

In-situ observation

A laser profile scanner (Micro-Epsilon, scanCONTROL 2600-100) was used to measure the displacement of the top surface of the laminate during infusion (Figure 3). The frame ensured that the centerline of the laminate was directly under the sensor, to measure the thickness perpendicular to the ideal flow front. Given the sensor range, only the region at the corner, approximately 80 mm in either direction, was measured. The resin reservoir was attached to the side of the frame, to ensure no significant height difference between reservoir and inlet point. After curing, the part was demolded without moving the tool, and the laser profile scanner measured the corresponding position of the tool surface.

After demolding, laminates were sectioned along the centerline, polished, and imaged using a digital light microscope (Keyence VHX-5000). Pixel measurements from the micrographs were used to measure the thickness along the centerline.

Initial FEA simulation

The simulation software relies primarily on Darcy's Law [21], given in Equation (2), where v is flow velocity, $[K]$ is the permeability tensor, μ is dynamic viscosity, and ∇P is the pressure gradient. By

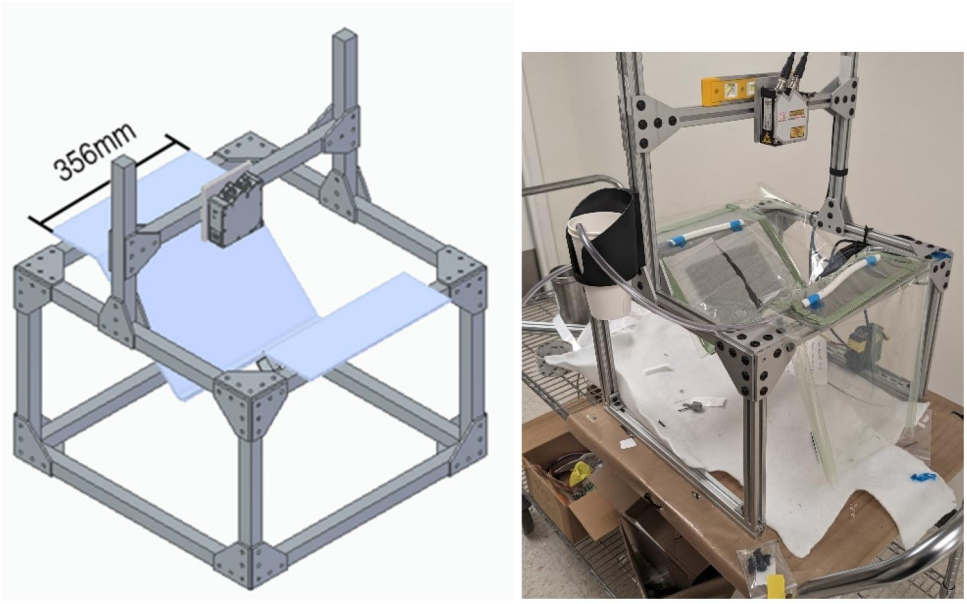

Figure 3. Experimental configuration for laminate infusion. (Left) Schematic of the laser displacement system. (Right) Experimental setup.

including mechanical coupling, the permeability tensor is recalculated and updated between calculation steps, thus accounting for the changes in fiber volume fraction [22]. While the software can also simulate heating and curing conditions, the present study concerns only the filling simulation.

$$v = \frac{[K]}{\mu} \nabla \mathrm{P} \tag{2}$$

The initial stage of this investigation encompassed a fluid-mechanical coupled finite element analysis (FEA, PAM-RTM). The fabric properties, listed in Table 1, served as input parameters for initial simulations. A constant resin viscosity of 0.3 Pa·s, measured *via* rheology, was applied. Inputs into the software included tool geometry, the number of plies, and the uncompressed thickness of the fabric, all of which were used in the development of a Laminate Mesh (LM) geometry. The laminate geometry for the LM approach involves setting the element size such that each ply is one element thick. Exploiting the flexibility inherent in the simulations, a broad range of tool geometries were selected, encompassing three diverse sets, detailed in Table 3. The outcomes from these simulations were used to extract thickness values through the node positions at the centerline of the top and tool surface.

All simulations maintained uniform processing conditions. Application of vacuum *via* the outlet edge was constant. Simultaneously, a uniform pressure was exerted on the top surface, ramping up to atmospheric pressure in a span of 90 s. Thereafter, this applied pressure was maintained. After 120 s, the inlet was opened at atmospheric pressure. Subsequently, the nodes on the tool surface were rigidly fixed, whereas the remaining nodes were constrained in-plane. The simulation culminated with complete saturation of the laminate.

Table 3. Tool geometries used in FEA.

Curvature [–]	Corner angle [°]	Corner radius [mm]
Set 1: Varying corner angle		
Flat	N/A	N/A
Concave	15/30/45/60/75/90	10
Convex	15/30/45/60/75/90	10
Set 2: Varying corner radius		
Flat	N/A	N/A
Concave	90	10/15/20/25
Convex	90	10/15/20/25
Set 3: Comparison to experimental trials		
Flat	N/A	N/A
Concave	90	10
Concave	60	10
Convex	90	15
Convex	60	15

Revised compaction and geometry

Results from the first round of simulations revealed the need for a refined methodology for predicting the final cured geometry (the simple assignment of tool geometry and generation of a laminate mesh was insufficient). There was deviation from the expected compaction behavior when the fabric was laid upon the tool: fabric bridging for the concave tools and fabric buckling for the convex tools. This realization prompted a series of tests to more accurately determine the compaction response and uncompacted geometry of the fabric on each tool.

Fabric was laid up on the tool and subsequently vacuum-sealed within a bag. A pair of pressure sensors (Composite Integration, XE-0050-008) were connected to the inlet and outlet lines. By controlling the vacuum level inside the bag, the top surface of the preform was measured using the laser

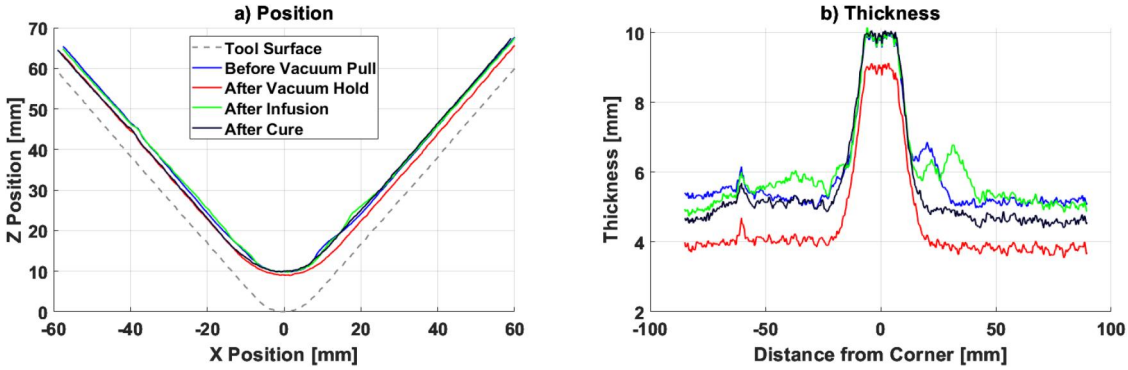

Figure 4. Position and thickness data during infusion with Tool B. (a) Laser sensor acquired position data. (b) Thickness data, derived from position data.

displacement sensor. The ply stack was placed under vacuum for a minimum of one hour. Then, the pressure level inside the bag was increased by 3400 Pa (1 inHg) in fixed intervals, allowing the fabric to stabilize before the next increment. When the pressure within the bag equaled atmospheric pressure, the process was reversed, increasing the vacuum level in fixed intervals and allowing the fabric to rest between intervals until maximum vacuum was reestablished.

Positional data from the laser displacement sensor was transformed to thickness data. Combined with pressure, a Thickness versus Pressure response curve was generated for each tool geometry for the intervals of steady pressure. Because the simulation software required uniform material properties, each geometry was segmented into *Flange, Corner,* and several *Edge* regions. From the Pressure versus Thickness data, a Stress versus Strain response was obtained for each region, with the multiple *Edge* regions being averaged into one. The data was subsequently fit to derive a stress-strain curve for the *Corner*, *Edge*, and *Flange* of each tool geometry. Based on previous experience with the software, exponential curves were used in the fitting.

The tool surface profile and the preform surface at full decompaction were measured and used to construct a set of User Defined Geometries (UDG). Curve fitting was performed to ensure preservation of symmetrical and smooth surfaces for simulations. The full curve was subsequently divided into appropriate regions for each tool geometry, with each assigned the Corner, Edge or Flange elastic properties and uncompressed volume fraction. Instead of generating the laminate mesh from individual ply properties, the UDG was used to generate a 3D solid, and then split into elements such that each ply was one element thick. The second set of simulations used the same processing conditions as the LM simulations, as described in the previous section.

Results and discussion

In-situ observation

The laser displacement system was used to monitor the top-surface position of the laminate during infusion, transforming the positional data into thickness data. Figure 4 shows a typical data set, for Tool B. In Figure 4a, the primary difference arises for the 'After Vacuum Hold' curve, which reveals preform decompression during/after resin infusion. Inspecting thickness, Figure 4b more clearly shows the difference between the various points during infusion, revealing marked reduction in thickness, both at the corner and along flanks, after vacuum hold. Application of vacuum caused a decrease in thickness across the entire measurement domain, with the average thickness dropping 1.33 mm (±0.17) in the flange region and 0.84 mm (±0.05) in the corner region. Upon completion of infusion, the average thickness reverted nearly to the value prior to vacuum pull, increasing by 1.42 mm (±0.28) and 0.88 mm (±0.08) in the flange and corner regions, respectively. As the resin cured, the thickness changed due to cure shrinkage, dropping 0.40 mm (±0.19) in the flange and increasing by 0.07 mm (±0.07) in the corner.

The anticipated difference in thickness between corner and flange regions was noted even before initiating infusion. At all stages – prior, during, and post-infusion – the thickness at the corner exceeded the flange thickness by approximately 5 mm. Once infusion concluded, the corner thickness returned to the value prior to vacuum pull and remained constant post-cure without significant cure shrinkage. This finding indicates that infusion introduces less variability in the corner region thickness compared to the flange region.

Flat laminates produced with Tool A showed modest bag inflation, but no major pleating was necessary to achieve bag integrity. Parts produced on Tool A geometry exhibited the most compaction during vacuum pull, and least thickness increase

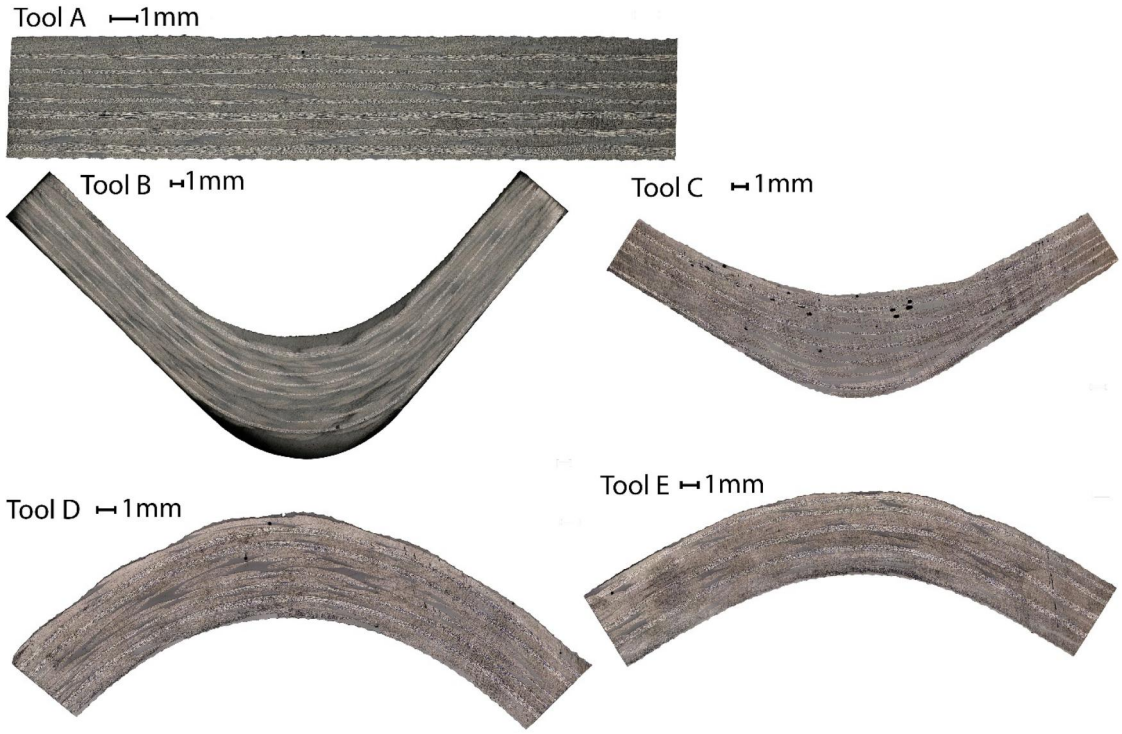

Figure 5. Micrograph of the cross-sections for the corner region for all five tool geometries. For Tool A, the center of the laminate is displayed. The tool side is facing downwards for all samples.

during filling. Given the small measuring area and the surface structure of the fabric, no significant thickness gradient was observed during infusion, aside from the expected decompression with the infusion of resin.

Analysis of polished sections

Cross-sections of the laminates at centerline are shown in Figure 5, with the tool-side facing down. Negligible porosity was observed in all parts, except for parts produced with Tool C, which exhibited voids in corner regions. The concave laminates produced with Tools B and C exhibited the morphology expected of concave corner parts – that is, fiber bridging, and increased thickness at the corner. Note that the fabric in Tool B did not completely fill the laminate and showed resin-rich regions on both the interior and exterior curve at the corner. Convex laminates revealed no significant defects, and laminates produced with Tool E maintained constant thickness throughout. Tow waviness was observed at the corner region in laminates produced with Tool D. Based on dry fabric compaction observations, this phenomenon can be attributed to buckling and bunching of the fabric at the corner during layup.

Simulation

Preliminary FEA simulation outcomes from the Laminate Mesh approach are presented in Figure 6. Two trends emerged from inspection, both of which were expected. First, sample thickness decreased from the inlet to the outlet side for all tool geometries (Figure 5, Tools A, B). The thickness gradient arises from the pressure difference between inlet and outlet. Second, parts with concave corners exhibited corner thickening, whereas those with convex corners exhibited corner thinning. As shown in Figure 6a, increasing the corner angle resulted in a larger maximum thickness deviation and a wider corner region The corner thickness deviation increased from 0.8% to 1.5% for concave parts and 0.5% to 0.8% for convex, while the corner width increases from 12.4 to 28.4 mm for concave parts and 11.7 to 25.6 mm for convex, respectively Conversely, Figure 6b shows that an increase in the corner radius decreased the thickness deviation at the corner, while expanding the corner region. Concave parts had the thickness deviation decrease from 1.5% to 0.5%, while convex parts decreased from 0.8% to 0.3%; corner width increased with corner radius, from 25.6 to 46.3 mm for both curvatures. These outcomes are consistent with expectations, with larger radius and corner angle both result in a larger tool arc, and a less sharp corner reduces pressure effects.

The thickness deviation at the corner was minor (0.3–1.5%) compared to the thickness deviation observed across the laminate length (16.8%). Even the sharpest corner geometry tested, a 10 mm 90° concave corner, exhibited a maximum deviation at the corner that was a small fraction (40%) of the

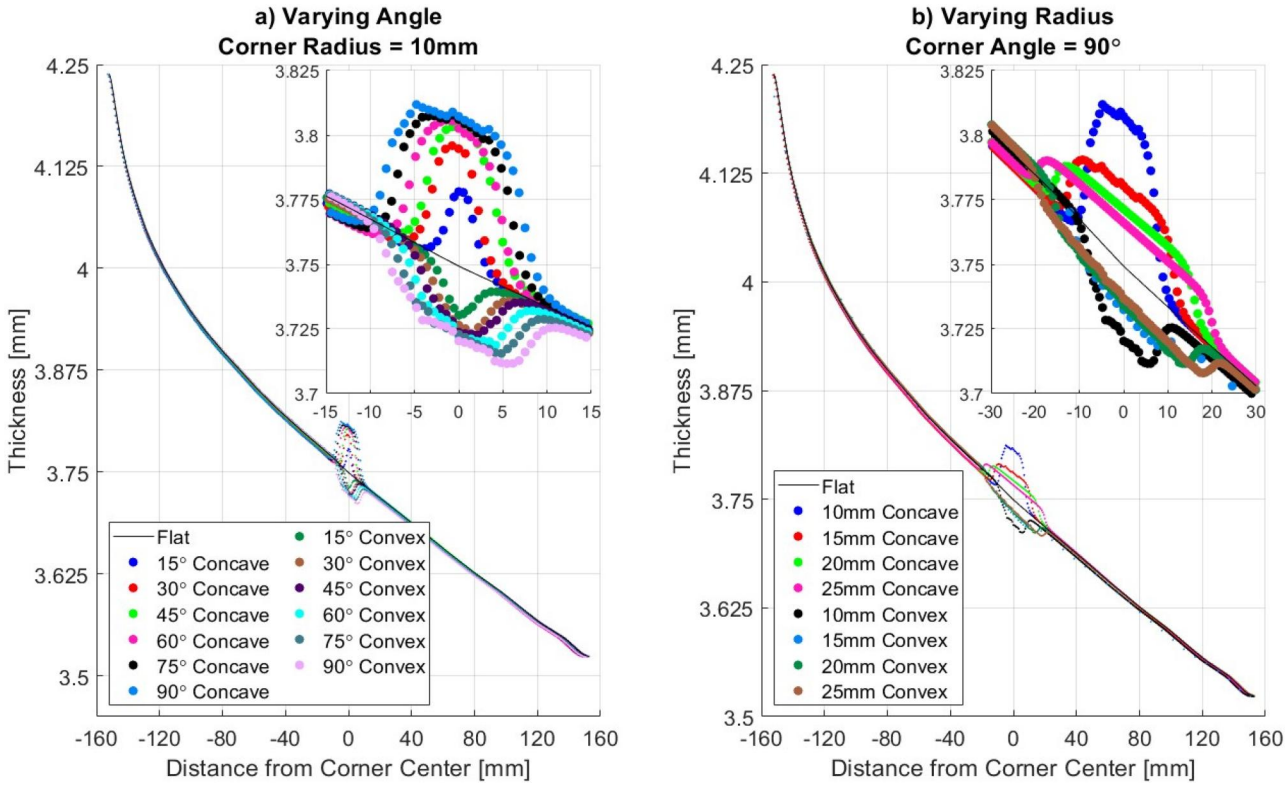

Figure 6. Thickness across the centerline of the laminates from FEA simulation using the laminate mesh. (a) Tool geometry set 1, varying corner angle; (b) tool geometry set 2, varying corner radius.

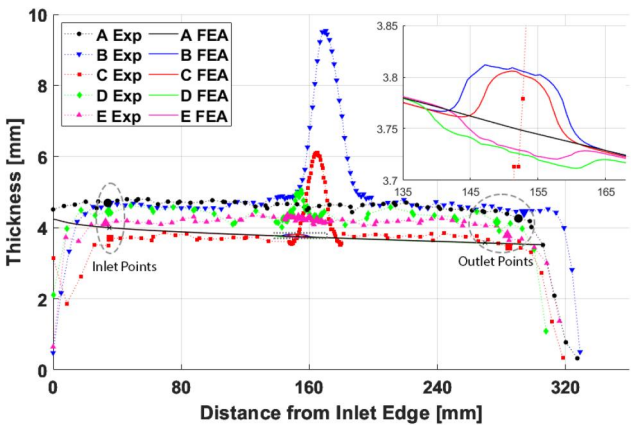

Figure 7. Thickness measurements of laminates centerline for all experimental trials, compared with FEA. The 'inlet' and 'outlet' points are indicated with enlarged markers. A zoomed-in look at the corner region of the FEA results is also shown.

thickness difference between inlet and outlet. Thickness measurements from laminates produced with Tools B and C (shown previously in Figure 4) showed a more pronounced thickness increase than predicted in simulations. In the following section, simulations of these conditions are compared to experimental results.

Thickness measurements

Cross-sectional measurements of laminate thickness revealed distinctive characteristics, and these findings were compared with the FEA results shown in Figure 7. Primarily, variations in thickness observed in the non-corner regions of the experimental parts were detected (both sides of central peak), and these were attributed to differences in fabric alignment and intrinsic reproducibility challenges associated with VI. Additionally, edge tapering was observed due to misaligned ply edges, arising from the contour radius changing as plies were laid down and shifting of the fabric at edges – an effect that was disregarded for this study. Hence, measurements 35 mm from either edge, defined as the 'inlet' and 'outlet' locations for subsequent analysis, are indicated in the graphs by the dashed circles. Minor waviness in the thickness curve was observed in all laminates, attributed to the fabric weave.

FEA results predicted a thickness difference of 0.71 mm between points 35 mm from the outlet and

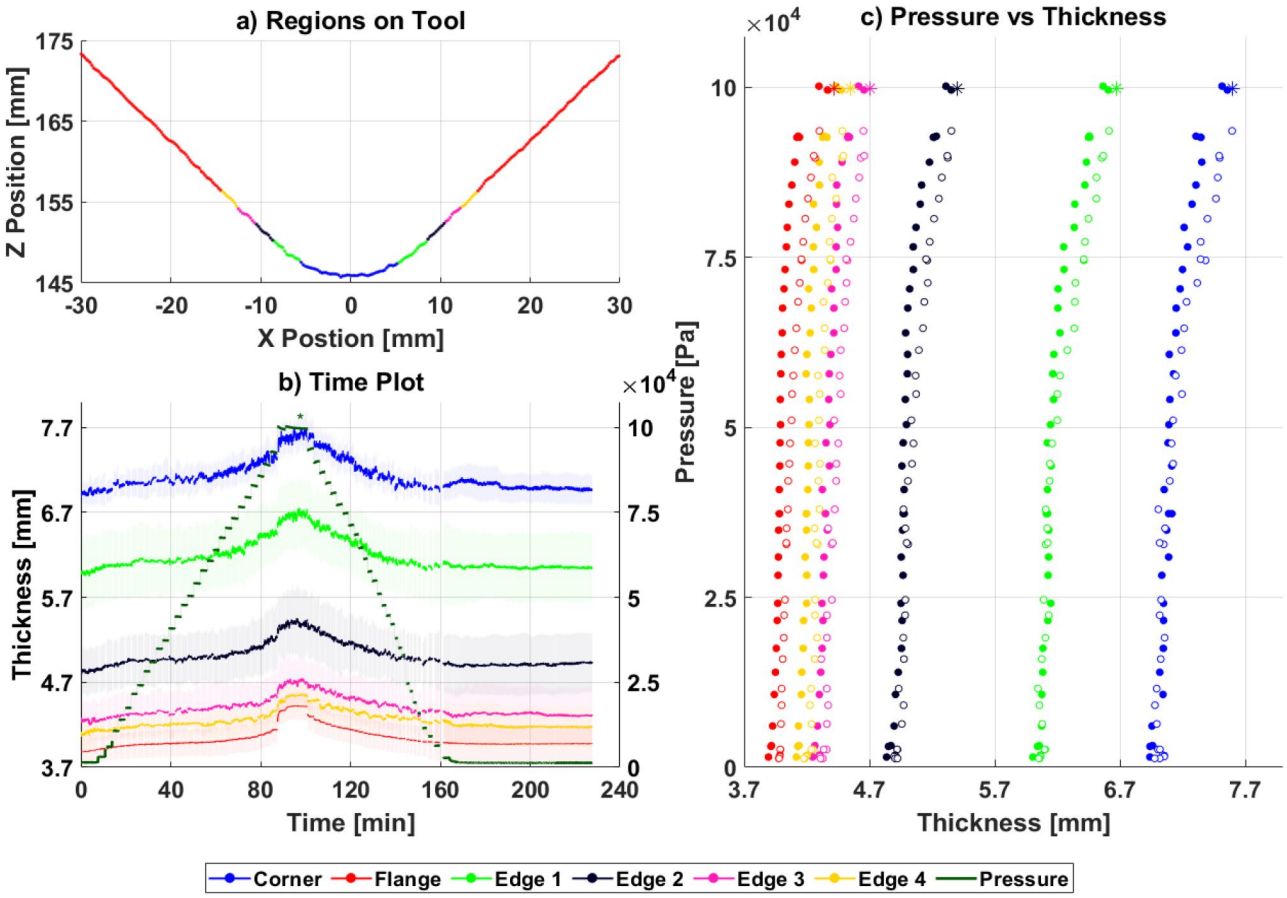

Figure 8. Process for obtaining the modified compaction results for Tool B. (a) Region positions labeled on Tool B; (b) average thickness of the different regions and pressure versus time; (c) thickness of the different regions versus pressure.

the inlet. The part produced using Tool A exhibited the most pronounced gradient and demonstrated a thickness difference of 0.48 mm, about 1/3 less than predicted. An inlet-outlet thickness gradient was not detected in experimental trials due to a combination of effects from thickness, waviness, and edges.

The trends in simulation results for corner regions generally aligned with cross-sectional observations. Concave laminates exhibited a thickness increase at the corner. In contrast, convex laminates exhibited only small variations in thickness. Tool D showed a minor increase in thickness, while Tool E presented negligible deviation in thickness at the corner. The sample showing maximum deviation, produced with Tool B, showed a corner-outlet difference of 5.1 mm, while the simulation predicted a much smaller thickness difference (0.27 mm, 18× less). The findings revealed a major limitation of simulations performed using the laminate mesh method. These simulations did not accurately predict the final thickness of contoured laminates produced *via* vacuum infusion.

Modified compaction response

The thickness of the corner region of the preform was measured during compaction and recompaction. The case for Tool B is shown in Figure 8. All regions followed a similar trend, with the rate of thickness increasing in a semi-exponential fashion during decompaction. During re-compaction, the thickness decreased more gradually. In general, the *Flange* region exhibited the lowest initial thickness and smallest thickness change, while the *Corner* region exhibited the greatest initial thickness and largest thickness change. The thickness of *Edge* regions fell between those of the *Corner* and *Flange*, and regions nearest the corner exhibited the largest thickness deviation. All of these results fall in line with expectations, with the fabric bridging, bending and bunching at the corner increasing the thickness while allowing for more space for compression, whereas the *Flange* region exhibits behavior much like the flat laminate, with the *Edge* regions forming a smooth transition between the two responses.

The compiled stress-strain curves for all tool geometries are illustrated in Figure 9. As expected, the *Corner* and *Edge* regions exhibited stiffer responses than the *Flange* region for all tools, and the Single Ply test and Tool A were more similar to the *Flange* region than the others, while still being less stiff. The contoured tools all exhibited similar responses in the *Edge* region, and likewise in the *Corner* region, except for Tool C, which showed a much

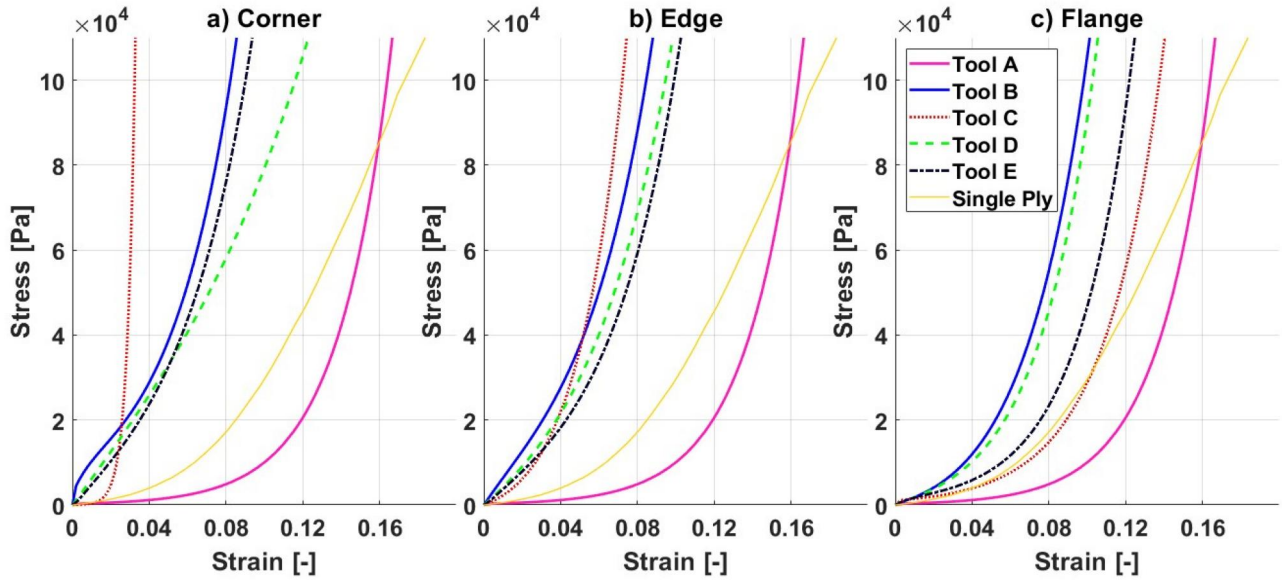

Figure 9. Modified compaction stress versus strain responses for the (a) corner, (b) edge, and (c) flange regions of each tool geometry. Also included is the single-ply stress versus strain response used in LM simulations.

stiffer response. The difference in Tool C was attributed to bridging of fibers, imparting increased stiffness. One might expect Tool B, which also exhibited bridging, to show a similar response; however, as shown in Figure 5B, the fabric did not fully conform to the corner, resulting in greater relaxation in corner compression during the pre-infusion stage. The stress-strain curves were then used as material properties for subsequent modified simulations.

Modified simulations

To impart greater accuracy to simulations, modified compaction response tests were deployed to develop a user defined geometry (UDG) for each tool. The tool-specific UDGs were used in modified simulations to generate predictions and compare with those obtained with conventional LM FEA. This UDG surface corresponded to the top surface profile of the preform, measured when the bag was at atmospheric pressure post-decompaction (denoted by an asterisk in Figure 8b). Curve-fitting and symmetry was assigned to the measured profiles to develop the UDG surface profiles, for compatibility with the software.

Figure 10 shows the measured surface profiles, together with the fitted curves employed for the UDG FEA simulations and the geometry developed using the LM method. The measured contours differ significantly from those generated by the LM method. For concave tools (Figure 10b, c), the LM simulation did not account for fabric bridging at the corner, behavior that was exhibited in the measured geometry and used in the UDG surface. While less pronounced, similar differences were observed in the convex tools (Figure 10d, e): the measured geometry showed a modest increase in thickness at the corner for Tool D, while Tool E showed a major deviation from the expected radial arc. In both cases, the deviations were attributed to fabric buckling and draping issues at the corner observed during layup. When laying down fabric on the convex tools, the innermost plies (closest to the tool), experienced compression, which is then transferred through the thickness. Tool E experienced the most compression, leading to minor fabric buckling, visible from the profile.

Thickness values generated by the UDG FEA simulations were obtained using the nodes at the centerline of the tool surface and the top surface, following the procedure used for the initial set of simulations. These results, plotted alongside the experimental measurements, are presented in Figure 11. A thickness gradient from inlet to outlet was again observed. However, unlike the LM simulations, the UDG simulations consistently demonstrated the expected corner thickening, which was attributed to the geometry of the uncompressed laminate, already displaying thickening due to the fiber effects during preform layup.

The thickness curve for Tool E did not conform to a smooth arc, unlike samples produced with other tools. This anomaly was attributed to deviation from a circular arc that was measured in the uncompressed fabric, illustrated in Figure 10e. Although this deviation was not observed in the laminate produced with Tool E, the thickness variation of Tool D showed a similar departure from the smooth arc.

Values of thickness deviations for relevant positions of the laminates are presented in Figure 12, shown as the % deviation from the thickness at the

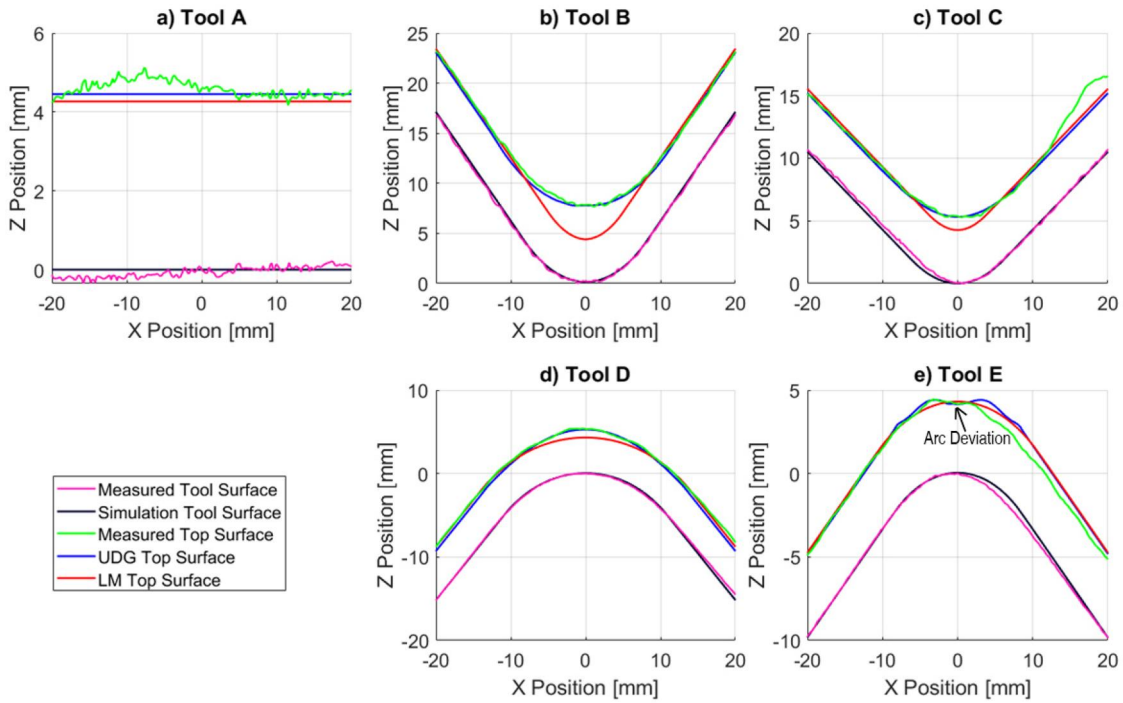

Figure 10. Measured, UDG and LM uncompressed surface profiles for the corner region of all tool geometries.

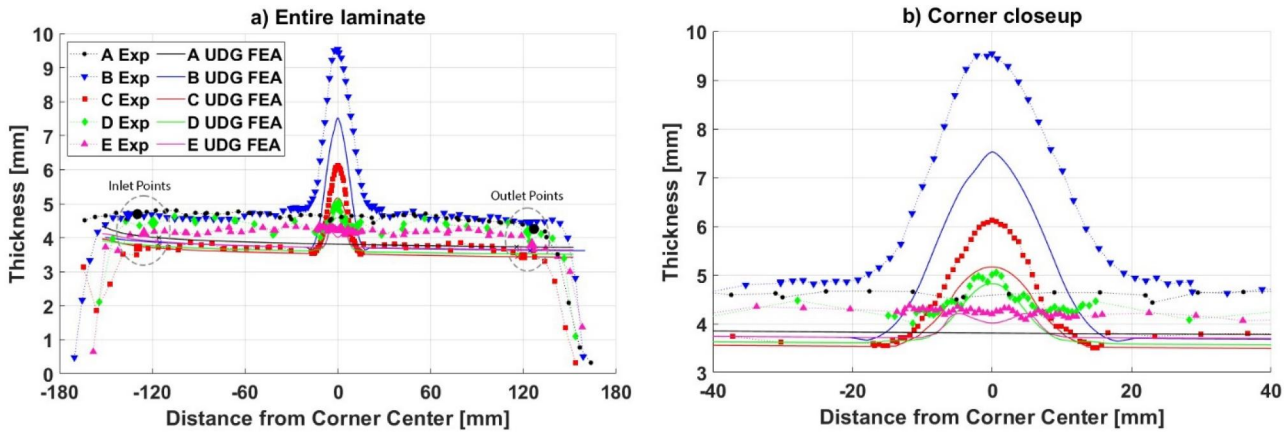

Figure 11. Thickness of UDG simulation vs. experimental results. (a) Plot showing the entire part length, with 'inlet' and 'outlet' points labeled, and (b) enlargement of the corner region.

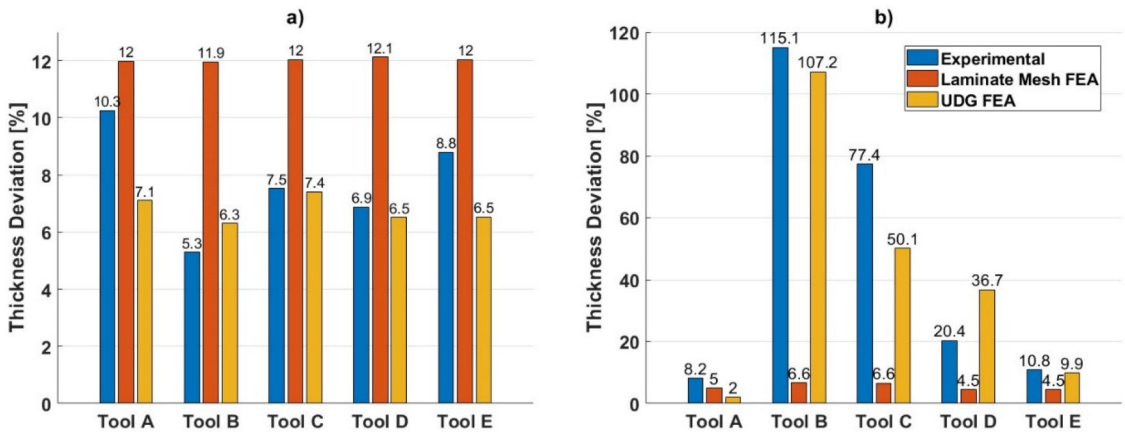

Figure 12. Thickness deviation between (a) the outlet and the inlet and (b) the outlet and the corner.

outlet. On average, LM simulations predicted a thickness deviation that was 0.28× experimental values at the corner, and 1.63× at the inlet, while the UDG simulations predicted a thickness deviation that on average was much closer to measured values (0.91×) at both corner and inlet. In general, the LM simulations overpredicted the general thickness deviation at the flange regions, and significantly under-predicted the corner thickness deviation. The UDG simulations predicted a thickness deviation that was much closer to measured values throughout the laminate length, within 30% in non-corner regions, and 20% elsewhere.

Comparing the experimental measurements to the UDG FEA simulations, greater accuracy was generally achieved in the region of laminate experiencing thickness deviation due to the corner, referred to as the corner width. For concave tools, UDG FEA simulations predicted a corner width 7% less (±4) than the measured value, while LM simulations were less accurate, predicting a width 43% less (±3) than measured. The width of the corner area of convex laminates was characterized by non-uniformity of the thickness distribution, and results of simulations contained apparent discrepancies. Notably, simulations consistently underpredicted the thickness of flange regions and of the flat laminate, Tool A. At the corner, the simulation predicted lower thickness for concave parts, and higher thickness for convex parts. These discrepancies arose from the difference in compaction effect once the fabric was saturated with resin. Resin saturation decreased the degree of compression of the laminate relative to dry compaction. The decrease was attributed to sharing of the compaction force between fabric and resin, affecting both overall thickness and thickness in concave regions. In addition, the presence of resin is expected to lubricate fibers, leading to nesting, allowing fabrics to conform to convex tools and reducing thickness, an effect not accounted for in FEA simulations.

In summary, a marked thickness deviation arose from corners in laminates produced *via* vacuum infusion, clearly outweighing thickness variations caused by the inherent pressure gradient. Material bridging at corners resulted in significant thickening and largely dictated the geometry of the contoured laminates. Minor thickness deviations were observed between the initial vacuum pull post-infusion and the fully cured stage. Despite a temporary thickness gradient emerging upon closure of the inlet and outlet, subsequent resin redistribution within the part yielded only a slight gradient across the contoured components. To account for the dominance of fiber bridging on thickness deviation, a solution was developed by measuring the post-layup geometry and using it as the starting geometry for the UDG FEA simulations. These modified simulations more closely matched the measured thickness values.

Conclusions

Process simulations were conducted to predict laminate thickness in parts with controlled corner geometry. To achieve accurate predictions, the method of assigning material properties was modified to account for fiber bridging at corners, resulting in deviation of <10% from experimental results. The results demonstrated a method for using commercial FEA simulation software to more accurate predict thickness deviations at corners. Refinements of this method can be integrated into commercial simulation codes and increase accuracy and utility. Most VI simulation codes today focus exclusively on resin flow, on achieving full saturation, and determining positions of inlet and outlet. The addition of mechanical effects in VI simulations can guide modification of pre-processing parameters and reduce thickness variations in cured laminates, thus achieving tighter tolerances. On the other hand, achieving greater accuracy in simulations also increases preproduction analysis time. Nevertheless, computation time is far cheaper than materials and labor, particularly for production of large parts.

While greater accuracy was achieved with the User Defined Geometry method than with the simple Laminate Mesh method, refinements to the method are required to further increase simulation fidelity. Alternative methods of segregating the corner region into distinct regions with different compaction response, or increasing the number of regions to achieve a more continuous effect within the simulations may also present advantages. Integration of draping simulations with finite element codes for VI process simulations can be leveraged to increase predictive accuracy of geometry features. For example, simulation of fabric draping during layup and initial vacuum pull will more accurately predict initial laminate geometry, which can be used as the UDG to simulate final part thickness, eliminating the need for post-layup fabric measurements. The present investigation focused only on the filling stage, neglecting potential geometric changes occurring during post-filling and curing. Such deviations were observed in experimental trials, and while minor, efforts to simulate such changes [23] are expected to be useful. FEA simulations may benefit from future efforts to gauge the wet compression response of fabrics. Finally, examination of specific responses for non-woven, unidirectional, or non-crimp fabrics is expected to

yield valuable insights and broaden utility of process simulations.

High areal weight fabrics are often used for vacuum infusion, but do not readily conform to sharp corners. Given that the pre-infused preform thickness distribution was shown to dominate the post-cured part thickness for concave parts, efforts to leverage techniques to increase uniformity during layup may be beneficial. As reported in previous studies, convex corners exhibit greater thickness uniformity than concave corners, and as such are preferred when possible. Methods to increase fabric-tool parity at corners, such as preform binders and pressure intensifiers, are almost mandatory, particularly in cases where large concave curvatures cannot be avoided.

Acknowledgements

The authors acknowledge undergraduate research assistants Ryan Kraemer and Ashiwini Balaganesh for their support in performing experiments. ESI is gratefully acknowledged for continuous support in our use of vacuum infusion simulation software.

Disclosure statement

No potential conflict of interest was reported by the authors.

ORCID

Patricio Martinez http://orcid.org/0000-0002-2588-4389

Data availability statement

The authors confirm that the data supporting the findings of this study are available within the article.

References

1. van Oosterom S, Allen T, Battley M, et al. An objective comparison of common vacuum assisted resin infusion processes. Compos Part A Appl Sci Manuf. 2019;125:105528. doi: 10.1016/j.compositesa.2019.105528.
2. Osborne T. An introduction to resin infusion. Reinf Plast. 2014;58(1):25–29. doi: 10.1016/S0034-3617(14)70038-4.
3. Tackitt KD, Walsh SM. Experimental study of thickness gradient formation in the vartm process. Mater Manuf Processes. 2005;20(4):607–627. doi: 10.1081/AMP-200041896.
4. Grofti Z, Croteau-Labouly B, Boukhili R, et al. Simultaneous characterization of preform expansion and permeability in vacuum assisted resin infusion. Polym Compos. 2022;43(6):3560–3573. doi: 10.1002/pc.26637.
5. Yenilmez B, Senan M, Murat Sozer E. Variation of part thickness and compaction pressure in vacuum infusion process. Compos Sci Technol. 2009;69(11-12):1710–1719. doi: 10.1016/j.compscitech.2008.05.009.
6. Levy A, Hubert P. Vacuum-bagged composite laminate forming processes: predicting thickness deviation in complex shapes. Compos Part A Appl Scid Manufact. 2019;126:105568. doi: 10.1016/j.compositesa.2019.105568.
7. Ma Y, Centea T, Nutt SR. Defect reduction strategies for the manufacture of contoured laminates using vacuum BAG-only prepregs. Polym. Compos. 2017;38(9):2016–2025. doi: 10.1002/pc.23773.
8. Fernlund G, Grif®th J, Courdji R, et al. Experimental and numerical study of the effect of caul-sheets on corner thinning of composite laminates. [Online]. www.elsevier.com/locate/compositesa.
9. Kozeny J. Uber Kapillare Leitung der Wasser in Boden. Royal Acad Sci Vienna Proc Class I. 1927;: 136:271–306. https://cir.nii.ac.jp/crid/1571417124968987776.bib?lang=en
10. Carman PG. Fluid flow through granular beds. Chem Eng Res Des. 1997;75(1 SUPPL):S32–S48. doi: 10.1016/S0263-8762(97)80003-2.
11. Bickerton S, Sozer EM, Advani SG. Fabric structure and mold curvature effects on preform permeability and mold filling in the RTM process. Part II. Predictions and comparisons with experiments. www.elsevier.com/locate/compositesa.
12. Trochu F, Ruiz E, Achim V, et al. Advanced numerical simulation of liquid composite molding for process analysis and optimization. Compos Part A Appl Sci Manufact. 2006;37(6):890–902. doi: 10.1016/j.compositesa.2005.06.003.
13. Adhikari D, Gururaja S, Hemchandra S. Vacuum infusion in porous preform with different mould configurations: flow simulation and experimental validation. J Reinf Plast Compos. 2021;40(7-8):321–338. doi: 10.1177/0731684420960209.
14. Yang B, Jin T, Bi F, et al. Modeling the resin flow and numerical simulation of the filling stage for vacuum-assisted resin infusion process. J Reinf Plast Compos. 2014;33(21):1976–1992. doi: 10.1177/0731684414551039.
15. Govignon Q, Bickerton S, Kelly PA. Simulation of the reinforcement compaction and resin flow during the complete resin infusion process. Compos Part A Appl Sci Manuf. 2010;41(1):45–57. doi: 10.1016/j.compositesa.2009.07.007.
16. Maung PP, Htet TL, Malysheva GV. Simulation and optimization of vacuum assisted resin infusion process for large-sized structures made of carbon fiber-reinforced plastics. In *IOP Conference Series: Materials Science and Engineering*, Institute of Physics Publishing, Jan. 2020. doi: 10.1088/1757-899X/709/2/022041.
17. Martinez P, Jin B, Nutt S. Permeability of multiaxial and Non-Crimp fabrics for vacuum infusion. In *Composites and Advanced Materials Expo*, Anaheim, Oct. 2022.
18. Chan AW, Hwang S. Anisotropic in-Plane permeability of fabric media. Polym Eng Sci. 1991;31(16): 1233–1239. doi: 10.1002/pen.760311613.
19. Arbter R, Beraud JM, Binetruy C, et al. Experimental determination of the permeability of

textiles: a benchmark exercise. Compos Part A Appl Sci Manuf. 2011;42(9):1157–1168. doi: 10.1016/j.compositesa.2011.04.021.

20. Vernet N, Ruiz E, Advani S, et al. Experimental determination of the permeability of engineering textiles: benchmark II. Compos Part A Appl Sci Manuf. 2014; 61:172–184. doi: 10.1016/j.compositesa.2014.02.010.
21. Darcy H. Les fontaines publiques de la ville de Dijon. Paris: Dalmont, 1856.
22. ESI Group. Private communication. 2019.
23. Caglar B, Yenilmez B, Sozer EM. Modeling of post-filling stage in vacuum infusion using compaction characterization. J Compos Mater. 2015;49(16): 1947–1960. doi: 10.1177/0021998314541305.